Electronic Supplementary Material

N-Dopants Optimize the Utilization of Spontaneously Formed Photocharges in Organic Solar Cells

Yabing Tang,[a] Hong Zheng, [b] Xiaobo Zhou,[a] Zheng Tang, [c] Wei Ma,[a] and Han Yan*[a]

[a]State Key Laboratory for Mechanical Behavior of Materials, School of Materials Science and Engineering, Xi'an Jiaotong University, Xi'an 710049, China. E-mail: mseyanhan@xjtu.edu.cn
[b]Center of Nanomaterials for Renewable Energy, State Key Laboratory of Electrical Insulation and Power Equipment, School of Electrical Engineering, Xi'an Jiaotong University, Xi'an 710049, China
[c]Center for Advanced Low-dimension Materials, State Key Laboratory for Modification of Chemical Fibers and Polymer Materials, College of Materials Science and Engineering, Donghua University, Shanghai 201620, China

Experimental Section

Materials. PM6, BTP-eC9, IEICO, ITIC and Poly [(9,9-bis(3'-(N,NdiMethyl)-NethylaMMoiniuM-propyl)-2,7-fluorene)-alt-2,7-(9,9–dioctylfluorene)]dibromide (PFN-Br) were purchased from Solarmer Materials Inc. Y6 was purchased from eFlexPV Inc. N-DMBI, Chloroform (CF), methanol and CuSCN were purchased from Sigma-Aldrich. TBAI and 1-Chloronaphthalene (CN) was purchased from TCI. Diethyl sulfide (DES) was purchased from Meryer. Phen-NaDPO was purchased from Zhengzhou Alfachem Inc. Ethanol was purchased from Acros organics. 1,3-dibromo-5-chlorobenzene (DBCl) was purchased from TCI. 3,3'-(1,3,8,10-Tetraoxoanthra[2,1,9-def:6,5,10-d'e'f']diisoquinoline-2,9(1H,3H,8H,10H)-diyl)bis(N,N-dimethylpropan-1-amine oxide) (PDINO) was purchased from Vizuchem. All chemicals were used as received without further purification. L8-BO was purchased from Hyper, Inc. DMBI-BDZC was purchased from Strem Chemicals, Inc.

Instrumentation. TM-AFM images were scanned by Bruker Dimension Icon in a tapping mode. The *J–V* curves were performed in the N_2-filled glovebox under AM 1.5G (100 mW cm^{-2}) using an AAA solar simulator (SS-F5-3A, Enli Technology Co., Ltd.) calibrated with a standard photovoltaic cell equipped with KG5 filter. The EQE curves were measured by Solar Cell Spectral Response Measurement System QE-R3018 (Enli Technology Co., Ltd.) with calibrated light intensity by a standard Si photovoltaic cell. PL spectra and temperature-dependent PL spectra for Y6 and PM6:Y6 (0.01:1) films were recorded by FLS980 spectrometer (Edinburgh Instruments, EI). The temperature was controlled by the OXFORD attachment. The PL spectra for L_{EX} calculation were recorded by Maya2000pro. The photostability is measurement under continuous illumination of Xenon lamp with a UV filter in nitrogen. The GIWAXS measurements were performed at beamline 7.3.3[1] at the Advanced Light Source. Samples were prepared on Si substrates using identical blend solutions as those used in devices. The 10 keV X-ray beam was incident at a grazing angle of 0.11°-0.15°. The scattered x-ray was detected using a Dectris Pilatus 2M photon counting detector.

The EQE_{EL} measurement system is consisted of a Keithley 2400 digital source meter, Keithley 6482 picoammeters and a standard Si detector (S1337-1010Br). For the sensitive EQE (sEQE) measurement, the light from halogen light source (LSH-75, Newport) becomes monochromatic light by using a monochromator (CS260-RG-3-MC-A, Newport), and is focused on the device to generate electrical signals. Then the signals are amplified by the front-end current amplifier (SR570, Stanford) and finally collected by the phase-locked amplifier (Newport). The EQE spectrum was obtained by using the corrected Si standard detector (S1337-1010Br).

Device Fabrication. The dilute BHJ organic solar cell was fabricated in a traditional device structure of ITO/PEDOT:PSS (Heraeus Clevios PVP Al 4083)/active layer/ PFN-Br/Al. The patterned ITO substrates were sequentially cleaned by deionized

water, acetone, and isopropanol. Before the coating of PEDOT:PSS, the substrates were firstly treated by ultraviolet ozone for 20 min, and the PEDOT:PSS solution was spin-coated on ITO substrates with a speed of 5500 rpm for 30 s, followed by thermal annealing at 150 °C for 10 min. Then Y6 (20 mg/ml) with different proportions of N-DMBI and PM6 (6 mg/ml) were dissolved in CF solvent, and stirring on a hot plate at 50 °C for more than 2 hours. 1 wt% PM6 was added to Y6 solutions later to obtain blend solutions. After that, the solutions were spin-coated on PEDOT:PSS to obtain similar film thickness of 70 nm ± 10 nm. Then a thin PFN-Br layer (0.5 mg/mL in methanol, 3300 rpm for 30 s) was spin coated on the active layer. Finally, 100 nm Al was deposited at a vacuum level of < 5×10^{-4} Pa. Typical devices area (0.04 cm^2) was defined by a metal mask with aligned aperture.

For the fabrication of bilayer devices to calculate L_{EX+CS}, the patterned ITO substrates were firstly cleaned following the dilute BHJ devices. CuSCN (25 mg/ml) was dissolved in DES at 60 °C for 1 h and then filtered. Then the CuSCN solution was spin-coated on ITO substrates at 1500 rpm for 30 s, followed by annealing of the device at 105 °C for 10 min to obtain thin films with thickness of ca. 60 nm. Y6 was dissolved in CF with different concentrations (3-20 mg/ml) and was spin-coated on CuSCN layer at different speeds for 30 s to obtain film thicknesses ranging from 8 nm to 150 nm. Next, a layer of ca. 5 nm of Phen-NaDPO as electron-transport layer (ETL) and exciton blocking layer (EBL) was spin-coated from methanol solution (0.5 mg/ml) on top of the Y6 layer. Finally, 100 nm Al was deposited at a vacuum level of < 5×10^{-4} Pa. Typical devices area (0.04 cm^2) was defined by a metal mask with aligned aperture.

The sequential deposited BHJ film was fabricated in the aforementhioned traditional device structure with altered interfacial layer of PDINO (2 mg/mL in methanol, 3300 rpm for 30 s). To fabricate 100 nm thin blend film, Y6/DBCl (1:2, 30 mg/ml in total) with different proportions of N-DMBI and PM6 (10 mg/ml) were dissolved in CF solvent and stirring on a hot plate at 50 °C for more than 2 hours. After that, the PM6 solution was firstly spin-coated on PEDOT:PSS to obtain film thickness of 50 nm, and then the Y6/DBCl/N-DMBI blend solution was spin-coated on PM6 film at 4000 rpm for 30s to obtain film thickness of 100 nm. To fabricate 300 nm thick blend film, Y6/DBCl (1:2, 45 mg/ml in total) with different proportions of N-DMBI and PM6 (15 mg/ml) were dissolved in CF solvent and stirring on a hot plate at 50 °C for more than 2 hours. After that, the PM6 solution was firstly spin-coated on PEDOT:PSS to obtain film thickness of 130 nm, and then the Y6/DBCl/N-DMBI blend solution was spin-coated on PM6 film 2500 rpm for 30s to obtain film thickness of 300 nm. To fabricate 400 nm thick blend film, Y6/DBCl (1:2, 45 mg/ml in total) with different proportions of N-DMBI and PM6 (15 mg/ml) were dissolved in CF solvent and stirring on a hot plate at 50 °C for more than 2 hours. After that, the PM6 solution was firstly spin-coated on PEDOT:PSS to obtain film thickness of 180 nm, and then the Y6/DBCl/N-DMBI blend solution was spin-coated on PM6 film at 1300 rpm for 30s to obtain film thickness of 400 nm. The PM6 : Y6 BHJ devices were fabricated in the aforementhioned traditional device structure with altered interfacial layer of PDINO and in the inverted structure of ITO/ZnO/active

layer/MoO_3/Al. ZnO was deposited by spin-coating a ZnO precursor solution (zinc acetate dihydrate, dissolved in 2-Methoxyethanol with Ethanolamine) at 5000 rpm for 1 min, followed by thermal annealing at 200 °C for 1 h. The active layer is fabricated by spin-coating PM6:Y6:DBCl (1:1.2:2.4 mg/ml, 33 mg/ml in total dissolved in CF solvent) blend solution with different proportions of N-DMBI on PEDOT:PSS/ZnO at 3300 rpm for 30s to obtain film thickness of 100 nm. 10 nm MoO_3 was deposited at a vacuum level of < 5×10^{-4} Pa. A thermal annealing at 80 °C for 5 min was performed for all the BHJ films here. The single-component Y6 devices were fabricated in the aforementhioned traditional device structure. Y6 (20 mg/ml) with different proportions of N-DMBI were dissolved in CF solvent, and stirring on a hot plate at 50 °C for more than 2 hours. After that, the solutions were spin-coated on PEDOT:PSS at 2000 rpm for 30s.

Calculating the exciton binding energy:

The Y6-Y6 dimer was constructed according to one previous report,[2] in which π-π stacking exists between the two Y6 complexes. In the Y6-$Y6H^-$/N-$DMBI^+$ structure, the N-$DMBI^+$ molecule is located above the stacking area of the Y6-Y6 dimer. In geometrical optimization, the Y6-Y6 and Y6-$Y6H^-$/N-$DMBI^+$ structures were calculated with the ωB97XD functional.[3] the LanL2DZ basis set with the Los Alamos effective core potentials (ECPs) was used for the S atoms,[4] while the splitting valence basis set with one polarization function 6-31G(d) was used for other atoms.[5-7] Specially, before the calculation of the Y6-$Y6H^-$/N-$DMBI^+$ structure, we firstly calculated two types of Y6-$Y6H^-$ structure. In the Y6 dimer, there are two types of carbonyl groups. One is in the central π-π stacking area of the Y6 species and the other is far from the π-π stacking area. We chose the one with lower energy, in which the hydrogenation occurs in the carbonyl group far from the π-π stacking area, as the precursor of the Y6-$Y6H^-$/N-$DMBI^+$ structure.

The exciton binding energy (E_b) was evaluated as follow:[8-12]

$$E_b = IP - EA - E_g^o \quad \text{(S1)}$$

where E_g^o represents the optical gap (S1 state), which was obtained by TDDFT calculation at the ωB97XD/6-31G(d)~LanL2DZ level of theory. IP and EA represent the first vertical ionization potential and first vertical electron affinity, respectively. These two terms were evaluated according to the definitions of first IP and EA:

$$IP = E(A^+) - E(A),\ EA = E(A) - E(A^-)$$

where E(A) represents the electronic energy of a neutral molecule A. A^+ and A^- represent the electronic energies of +1 and -1 valence states of A, respectively.

All the DFT calculations were conducted with the Gaussian16 package.[13]

Calculating the energy loss:[14-15]

The total energy loss is composed of three parts as is shown by

$$q\Delta V_{loss} = E_g^{PV} - qV_{oc} \quad \text{(S2)}$$

$$= \left(E_g^{PV} - qV_{oc}^{SQ}\right) + \left(qV_{oc}^{SQ} - qV_{oc}^{rad}\right) + \left(qV_{oc}^{rad} - qV_{oc}\right)$$

$$= \left(E_g^{PV} - qV_{oc}^{SQ}\right) + q\Delta V_{oc}^{rad,below\ gap} + q\Delta V_{oc}^{nrad}$$

where $\triangle V_{loss}$ is the total voltage loss, E_g^{PV} is the photovoltaic bandgap energy, V_{oc}^{SQ} is the maximum voltage deduced by the Shockley-Queisser, V_{oc}^{rad} is the open-circuit voltage when there is only radiative recombination, $\triangle V_{oc}^{rad,\ below\ gap}$ is the voltage loss of radiative recombination from the absorption below the bandgap, $\triangle V_{oc}^{nrad}$ is the voltage loss of non-radiative recombination. The E_g^{PV} is determined by

$$E_g^{PV} = \frac{\int_a^b EP(E)dE}{\int_a^b P(E)dE} \tag{S3}$$

where $P(E)=d\mathrm{EQE}_{PV}/dE$, EQE_{PV} is determined by the sEQE measurement, E is the photon energy, a and b are selected where $P(a) = P(b) = 0.5\max[P(E)]$.

In order to calculate the energy loss parameters, we should firstly understand where the losses are from. The V_{oc} of any type of solar cells is determined by the ratio between short circuit current (J_{sc}) and and dark saturation current (J_0), following this expression:

$$V_{oc} = \frac{k_B T}{q} \ln\left(\frac{J_{sc}}{J_0} + 1\right) \tag{S4}$$

where k_B is the boltzmann constant, T is the temperature, and q is the elementary charge. The expression for J_{sc} and J_0 are given by:

$$J_{sc} = q \cdot \int_0^\infty EQE_{PV}(E) \cdot \varphi_{AM1.5}(E)dE \tag{S5}$$

$$J_0 = \frac{q}{EQE_{EL}} \cdot \int_0^\infty EQE_{PV}(E) \cdot \varphi_{bb}(E)dE \tag{S6}$$

The expression for J_0 is the Rau's reciprocity relation, where EQE_{EL} is radiative quantum efficiency of the solar cell when charge carriers are injected into the device in dark, $\varphi_{AM1.5}$ is the AM1.5 standard solar spectrum and φ_{bb} is the black body spectrum.

When all the recombination is radiative (i.e. $\mathrm{EQE}_{EL} = 1$), J_0 is minimized, and V_{oc} is maximized:

$$J_0^{rad} = q \cdot \int_0^\infty EQE_{PV}(E) \cdot \varphi_{bb}(E)dE \tag{S7}$$

$$V_{oc}^{rad} = \frac{k_B T}{q} \ln\left(\frac{J_{sc}}{J_0^{rad}} + 1\right) = \frac{k_B T}{q} \ln\left(\frac{q \cdot \int_0^\infty EQE_{PV}(E) \cdot \varphi_{AM1.5}(E)dE}{q \cdot \int_0^\infty EQE_{PV}(E) \cdot \varphi_{bb}(E)dE} + 1\right) \tag{S8}$$

In the Shockley-Queisser theory, the general quantum efficiency $\mathrm{EQE}_{PV}^{SQ}(E)$ can be defined as follow:

$$\begin{cases} EQE_{PV}^{SQ}(E) = 1, E > E_g^{PV} \\ EQE_{PV}^{SQ}(E) = 0, E < E_g^{PV} \end{cases} \tag{S9}$$

Substituting general quantum efficiency $\mathrm{EQE}_{PV}^{SQ}(E)$ (equation S9) in equation S5 and S7, then we can get the short circuit current and and dark saturation current in the SQ limit

$$J_{sc}^{SQ} = q \cdot \int_{E_g^{PV}}^\infty \varphi_{AM1.5}(E)dE \tag{S10}$$

$$J_0^{SQ} = q \cdot \int_{E_g^{PV}}^{\infty} \varphi_{bb}(E) dE \quad \text{(S11)}$$

In the same way, we can calculate the value of the SQ open-circuit voltage limit, V_{oc}^{SQ}, according to equation S8

$$V_{oc}^{SQ} = \frac{k_B T}{q} \ln\left(\frac{J_{sc}^{SQ}}{J_0^{SQ}} + 1\right) = \frac{k_B T}{q} \ln\left(\frac{q \cdot \int_{E_g^{PV}}^{\infty} \varphi_{AM1.5}(E) dE}{q \cdot \int_{E_g^{PV}}^{\infty} \varphi_{bb}(E) dE} + 1\right) \quad \text{(S12)}$$

The difference between V_{oc}^{SQ} and V_{oc}^{rad} is due to that in the SQ theory, the band edge of the absorber is totally abrupt when calculating V_{oc}^{rad}, the band gap will be smeared out for the existence of charge transfer state absorption.

Therefore, we can deduce the voltage loss of radiative recombination below the gap

$$\Delta V_{oc}^{rad,below\ gap} = V_{oc}^{SQ} - V_{oc}^{rad} \quad \text{(S13)}$$

The voltage loss due to non-radiative recombination, $\triangle V_{oc}^{nrad}$, can be rewritten as

$$\Delta V_{oc}^{nrad} = V_{oc}^{rad} - V_{oc} = -k_B T E Q E_{EL} \quad \text{(S14)}$$

From which we can calculate the V_{oc} value. Based on the previous discussions, we are now able to summarize the energy loss from the E_g^{PV} to the qV_{oc} for any type of solar cells. We can get these three terms of energy losses based on related experiments and calculations.

Calculating the L_{EX}:[16-18]

The one-dimensional exciton diffusion equation, without considering the contribution of FRET and bimolecular exciton deactivation processes such as singlet-singlet, singlet-triplet, and singlet-polaron annihilations, can be simplied as:

$$\frac{\partial n(x,t)}{\partial t} = D \frac{\partial^2 n(x,t)}{\partial x^2} + G(x,t) - \frac{n(x,t)}{\tau} \quad \text{(S15)}$$

where $n(x,t)$ is the time-dependent exciton density at position x in the organic film, D is the diffusion coefficient, $G(x,t)$ is the time-dependent exciton generation profile at position x, the third term of the right-hand side represents exciton deactivation via the radiative and nonradiative decays. Considering the boundary conditions of complete exciton quenching at Y6/CuSCN interface (n=0) and complete exciton reflection at Y6/air interface ($\partial n/\partial x$=0), the PL quenching efficiency (Φ_q) is calculated as a function of Y6 thickness (x_0), exciton diffusion length (L_{EX}) and the absorption coefficient (α, the optical field is simply assumed to decrease exponentially along the propagation direction) as follows:

$$\Phi_q(x_0, L_{EX}, \alpha) = 1 - \frac{\int_0^{\infty} \int_0^{x_0} n(x,t,L_{EX},\alpha) dx dt}{\int_0^{\infty} \int_0^{x_0} n_{ref}(x,t,L_{EX}) dx dt} =$$

$$\frac{\left[\alpha^2 L_{EX}^2 + \alpha L_{EX} \tanh\left(\frac{x_0}{L_{EX}}\right)\right] exp(-\alpha x_0) - \alpha^2 L_{EX}^2 \left[\cosh\left(\frac{x_0}{L_{EX}}\right)\right]^{-1}}{(1-\alpha^2 L_{EX}^2)[1-exp(-\alpha x_0)]} \quad \text{(S16)}$$

where n and n_{ref} are the exciton density with and without the quenching layer, respectively. Under the uniform excitation condition across optically thin films, the PL ratio can be simplified as:

$$\frac{PL_{Y6/CuSCN}}{PL_{Y6}} = 1 - \Phi_q(x_0, L_{EX}) = 1 - \frac{L_{EX}}{x_0} \tanh\left(\frac{x_0}{L_{EX}}\right) \quad \text{(S17)}$$

where $PL_{Y6/CuSCN}$ is the integrated PL intensity of Y6/CuSCN bilayer film, PL_{Y6} is the integrated PL intensity of Y6 film.

Calculating the L_{EX+CS}:[19-21]

According to previous reports, the EQE spectra of the bilayer devices with a series acceptor film thicknesses can be modeled with the well-known one-dimensional exciton diffusion equation:

$$\frac{\partial n(x,t)}{\partial t} = D\frac{\partial^2 n(x,t)}{\partial x^2} + G(x,t) - k_{PL}n(x,t) - k_{FRET}n(x,t) - \gamma n(x,t)^2 \quad \text{(S18)}$$

where G(*x*,*t*) is the time-dependent exciton generation profile at position x given by transfer-matrix modeling, k_{PL} is the radiative decay rate without quencher sites, γ is an exciton-exciton annihilation rate constant, and k_{FRET} denotes the rate of Förster resonance energy transfer (FRET) in the presence of a neighboring material.

It is worth noting that FRET between CuSCN and Y6 is negligible owing to the small overlap of CuSCN's absorption with Y6's emission, so k_{FRET} is zero. Due to the small light intensity during EQE measurements, exciton-exciton annihilation rate constant (γ) is also regarded as zero. Hence, Eq. (2) can be simplified under steady-state conditions with

$$k_{PL} = \frac{D}{L_{EX+CS}^2} \quad \text{(S19)}$$

as

$$\left(\frac{\partial^2}{\partial x^2} - \frac{1}{L_{EX+CS}^2}\right) n(x) = -\frac{G(x)}{D} \quad \text{(S20)}$$

where L_{EX+CS} is the exciton and CS transport length calculated by EQE method. It's general solution can be written as:

$$Dn(x) = \left[k_1 - \frac{L_{EX+CS}}{2}\int_{x_0}^{x} e^{-\hat{x}/L_{EX+CS}}G(\hat{x})d\hat{x}\right]e^{x/L_{EX+CS}} + \left[k_2 + \frac{L_{EX+CS}}{2}\int_{x_0}^{x} e^{\hat{x}/L_{EX+CS}}G(\hat{x})d\hat{x}\right]e^{-x/L_{EX+CS}} \quad \text{(S21)}$$

where k_1 and k_2 are constants and can be solved with boundary conditions of complete exciton quenching at Y6/CuSCN interface (n=0) and complete exciton reflection at Y6/Phen-DPO interface ($\partial n/\partial x$=0). So they are given as:

$$k_1 = -k_2 e^{-\frac{2x_0}{L_{EX+CS}}} \quad \text{(S22)}$$

$$k_2 = \frac{-\frac{L_{EX+CS}}{2}\int_{x_0}^{0} e^{-\hat{x}/L_{EX+CS}}G(\hat{x})d\hat{x} - \frac{L_{EX+CS}}{2}\int_{x_0}^{0} e^{\hat{x}/L_{EX+CS}}G(\hat{x})d\hat{x}}{\left(e^{-\frac{2x_0}{L_{EX+CS}}}+1\right)} \quad \text{(S23)}$$

The EQE can then be calculated considering that the photocurrent is only due to the exciton dissociation at the CuSCN/Y6 interface:

$$EQE = \frac{J_{photo}}{J_{inc}} = \frac{q\eta_c D}{J_{inc}}\frac{\partial n(x)}{\partial x}\bigg|_{interface} \quad \text{(S24)}$$

where J_{photo} and J_{inc} are the generated photocurrent density and the incident light current density. And the shape of normalized EQE vs. thickness data is only determined by $D\partial n(x)/\partial x$, which is given by

$$D\frac{\partial n(x)}{\partial x}(x = x_0) = \frac{1}{L_{EX+CS}}e^{x/L_{EX+CS}}k_1 - \frac{1}{L_{EX+CS}}e^{-x/L_{EX+CS}}k_2 \quad \text{(S25)}$$

The calculation is written in MATLAB language.

Calculating the SCLC mobility:

The SCLC mobility (μ) was measured with the hole-only device structure of ITO/PEDOT:PSS/active layer/MoO_3/Al and electron-only device structure of ITO/ZnO/active layer/PFN-Br/Al. The values of SCLC mobility were obtained by fitting the current density-voltage curves according to

$$J = \frac{9\varepsilon_0\varepsilon_r\mu V^2}{8d^3} \quad \text{(S26)}$$

where ε_0 is the permittivity of vacuum, ε_r is the relative permittivity of the active layer and it is assumed to be 3 here.

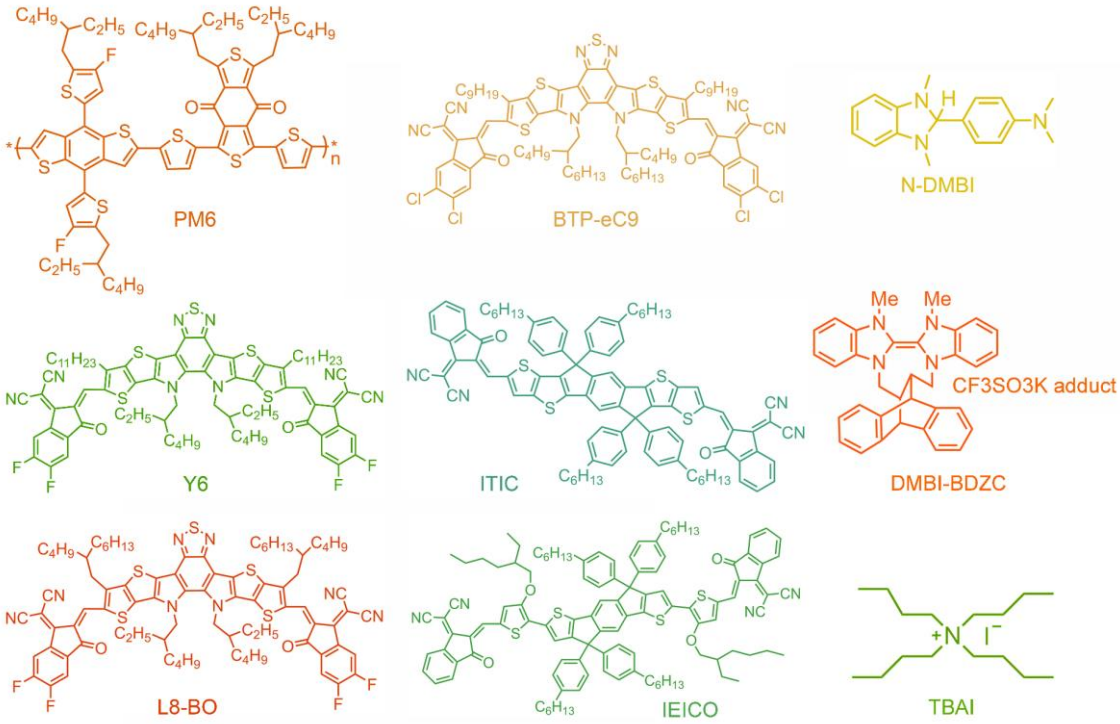

Fig. S1. The chemical structures of PM6, Y6, (2,2′-((2Z,2′Z)-((3,9-bis(2-butyloctyl)-12,13-bis(2-ethylhexyl)-12,13-dihydro-[1,2,5]thiadiazolo[3,4-e]thieno[2″,3″:4′,5′]
thieno[2′,3′:4,5]pyrrolo[3,2-g]thieno[2′,3′:4,5]thieno[3,2-b]indole-2,10-diyl)bis(methaneylylidene))bis(5,6-difluoro-3-oxo-2,3-dihydro-1H-indene-2,1-diylidene))dimalononitrile) (L8-BO), 2,2'-[[12,13-Bis(2-butyloctyl)-12,13-dihydro-3,9-dinonylbisthieno[2″,3″:4′,5′]thieno[2′,3′:4,5]pyrrolo[3,2-e:2′,3′-g][2,1,3]benzothiadiazole-2,10-diyl]bis[methylidyne(5,6-chloro-3-oxo-1H-indene-2,1(3H)-diylidene)]]bis[propanedinitrile] (BTP-eC9), 2,2'-[[6,6,12,12-tetrakis(4-hexylphenyl)-s-indacenodithieno[3,2-b]thiophene]methylidyne(3-oxo-1H-indene-2,1(3H)-diylidene)]]bis(propanedinitrile) (ITIC), 2,2′-((2Z,2′Z)-((5,5′-(4,4,9,9-tetrakis(4-hexylphenyl)-4,9-dihydros-indaceno[1,2-b:5,6-b′]dithiophene-2,7-diyl)bis(4-((2-ethylhexyl)-oxy)thiophene-5,2-diyl))bis(methanylylidene))bis(3-oxo-2,3-dihydro-1H-indene-2,1-diylidene))dimalononitrile (IEICO), N-DMBI,
(12a,18a)-5,6,12,12a,13,18,18a,19-Octahydro-5,6-dimethyl-13,18[1′,2′]-benzenobisbenzimidazo[1,2-b:2′,1′ d]benzo[i][2.5]benzodiazocine potassium triflate adduct (DMBI-BDZC) and tetrabutylammonium iodide (TBAI).

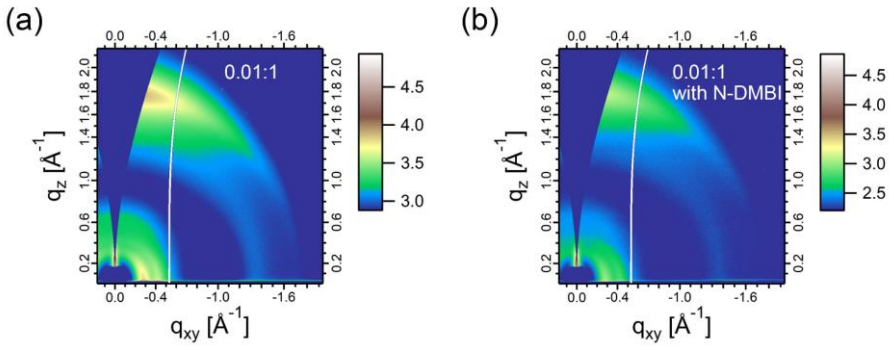

Fig. S2. (a-b) Two-dimensional GIWAXS scattering patterns of the pristine and 0.1 wt% N-DMBI added PM6:Y6 (0.01:1) films.

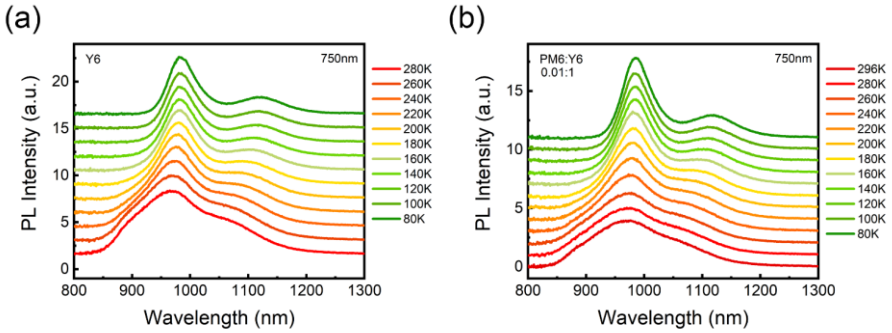

Fig. S3. (a) Temperature-dependent PL spectra for the Y6 film excited at 750 nm. (b) Temperature-dependent PL spectra for the PM6:Y6 (0.01:1) film excited at 750 nm.

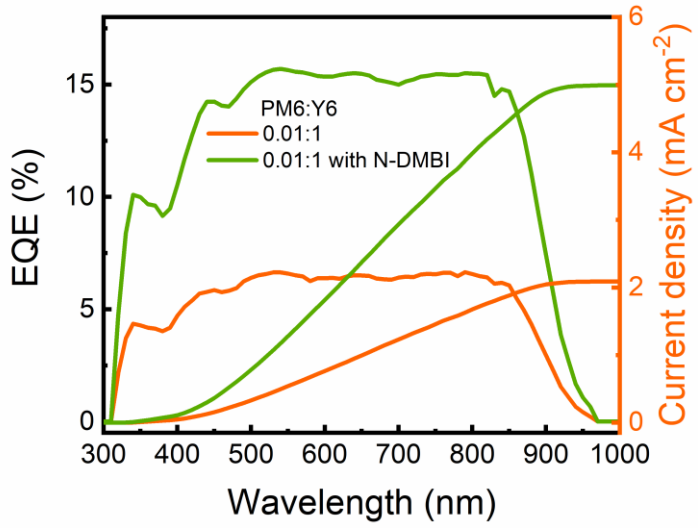

Fig. S4. EQE and corresponding integrated current density curves of the control and 0.1 wt% N-DMBI added PM6:Y6 (0.01:1) devices.

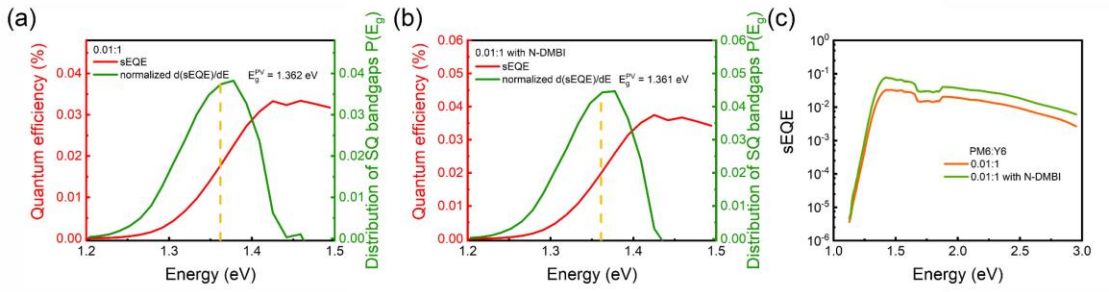

Fig. S5. (a-b) Photovoltaic band-gap energy (E_g^{PV}) of the control and 0.1 wt% N-DMBI added PM6:Y6 (0.01:1) devices. (c) sEQE spectra of the control and 0.1 wt% N-DMBI added PM6:Y6 (0.01:1) devices.

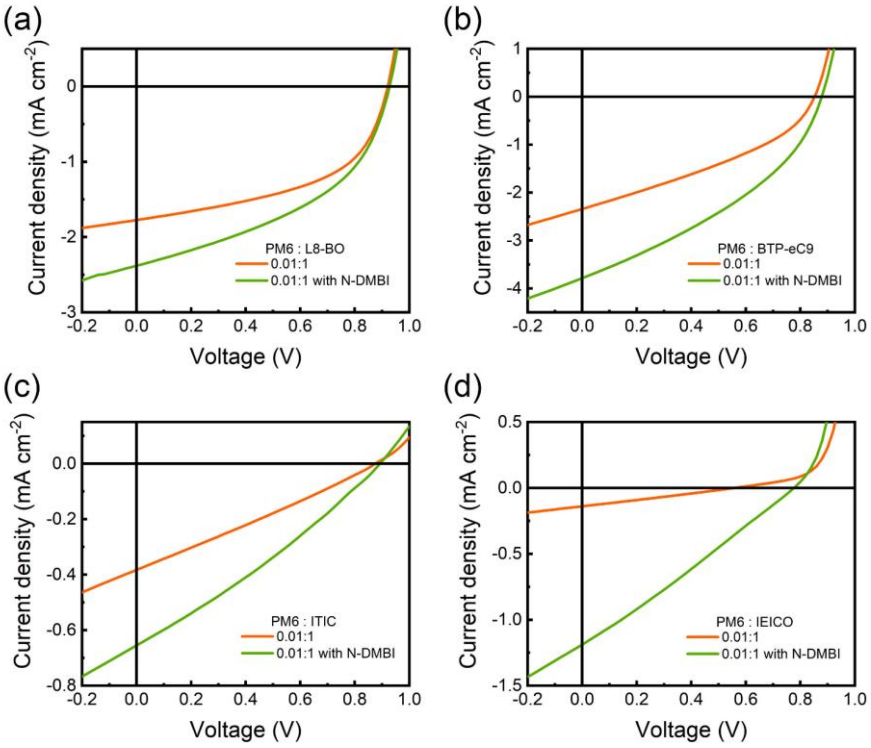

Fig. S6. (a) The *J-V* curves of the control and 0.05 wt% N-DMBI added PM6:L8-BO (0.01:1) devices. (b) The *J-V* curves of the control and 0.05 wt% N-DMBI added PM6:BTP-eC9 (0.01:1) devices. (c) The *J-V* curves of the control and 0.05 wt% N-DMBI added PM6:ITIC (0.01:1) devices. (d) The *J-V* curves of the control and 0.5 wt% N-DMBI added PM6:IEICO (0.01:1) devices.

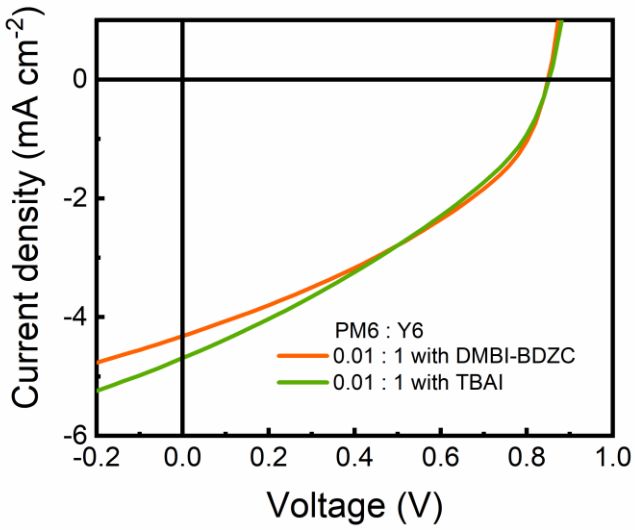

Fig. S7. The *J*-*V* curves of 0.1 wt% DMBI-BDZC added and 0.05 wt% TBAI added PM6 : Y6 (0.01:1) devices.

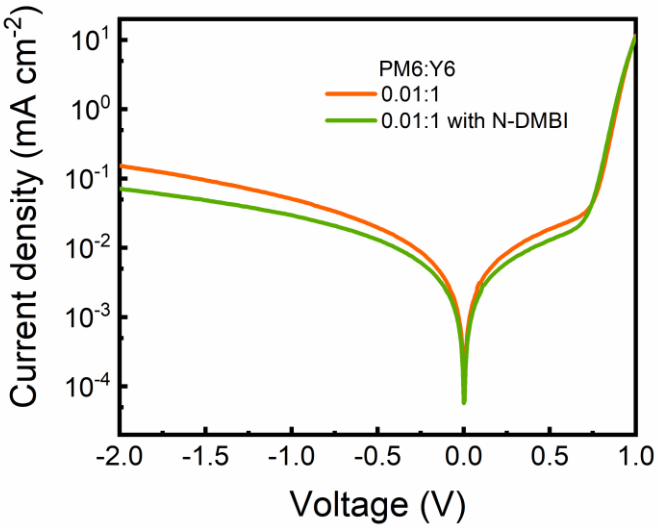

Fig. S8. Dark *J*-*V* curves of the control and 0.1 wt% N-DMBI added PM6:Y6 (0.01:1) devices.

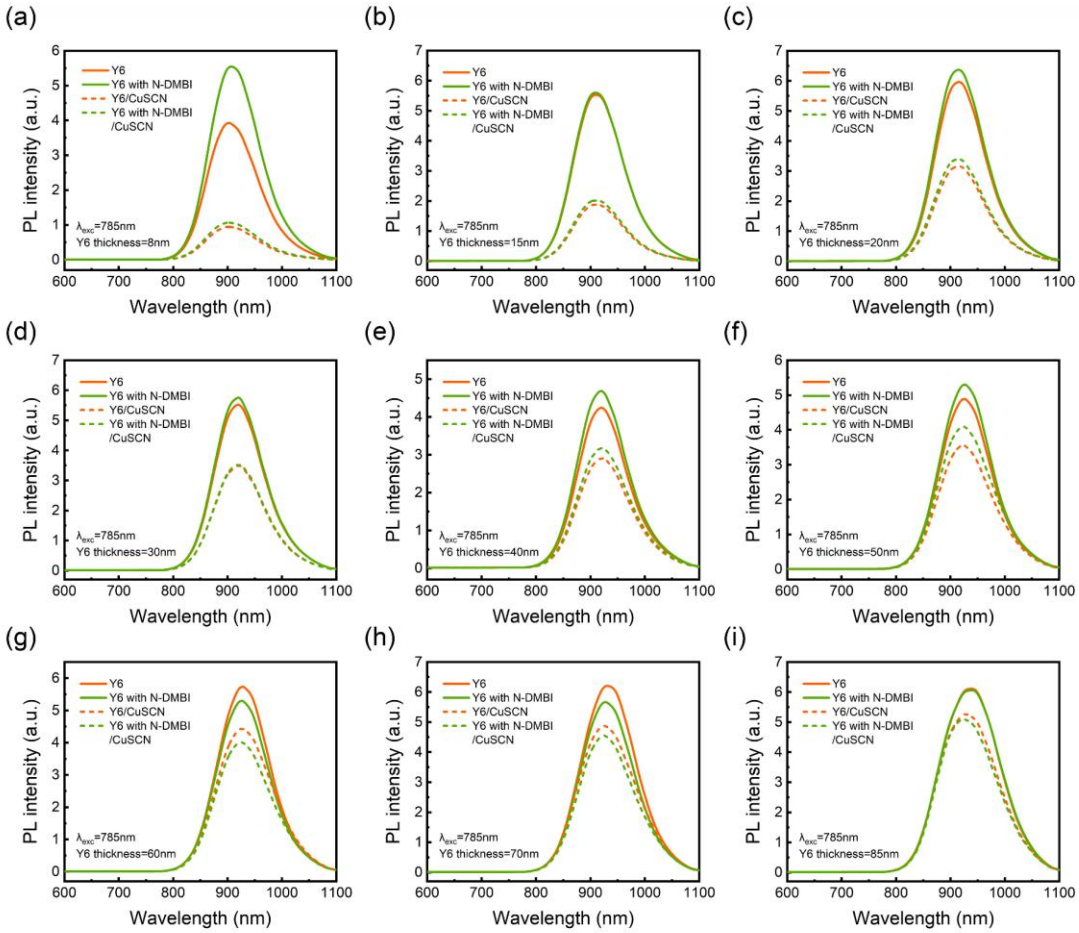

Fig. S9. (a-i) PL spectra of Y6, 0.1 wt% N-DMBI added Y6, Y6/CuSCN and 0.1 wt% N-DMBI added Y6/CuSCN films with various thicknesses (8 nm, 15 nm, 20 nm, 30 nm, 40 nm, 50 nm, 60 nm, 70 nm, 85 nm).

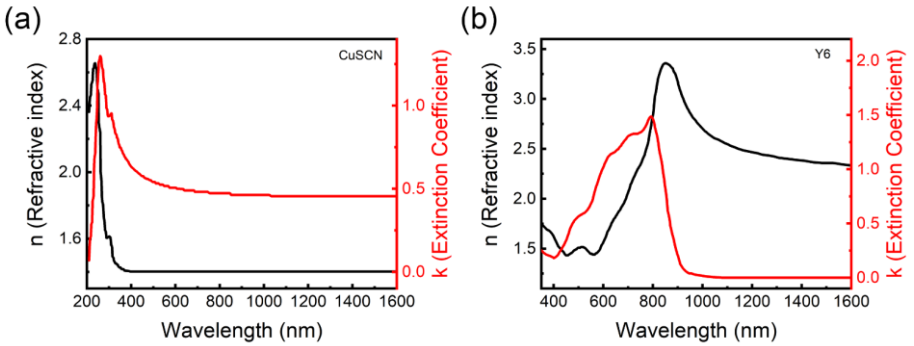

Fig. S10. (a-b) Refractive indexs and extinction coefficients of CuSCN[22] and Y6[23] films, respectively.

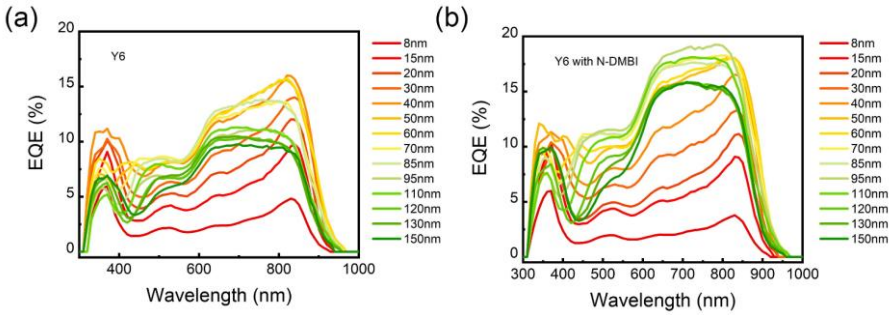

Fig. S11. (a) EQE spectra of Y6/CuSCN devices for different Y6 layer thicknesses. (b) EQE spectra of N-DMBI added Y6/CuSCN devices for different Y6 layer thicknesses.

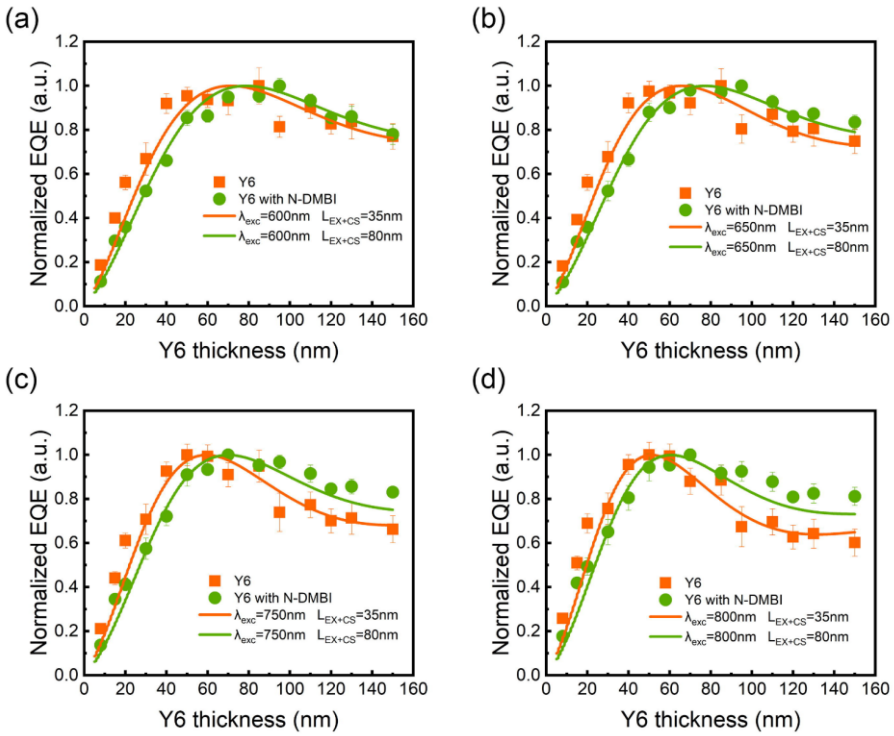

Fig. S12. L_{EX+CS} values from the thickness varying EQE measurements of the pristine and 0.1 wt% N-DMBI added CuSCN/Y6 bilayer devices. The excitation wavelength keeps at (a) λ_{exc} = 600 nm, (b) λ_{exc} = 650 nm, (c) λ_{exc} = 750 nm and (d) λ_{exc} = 800 nm. The experimental data (diamonds and circles) are fitted (solid lines) for all Y6 thicknesses.

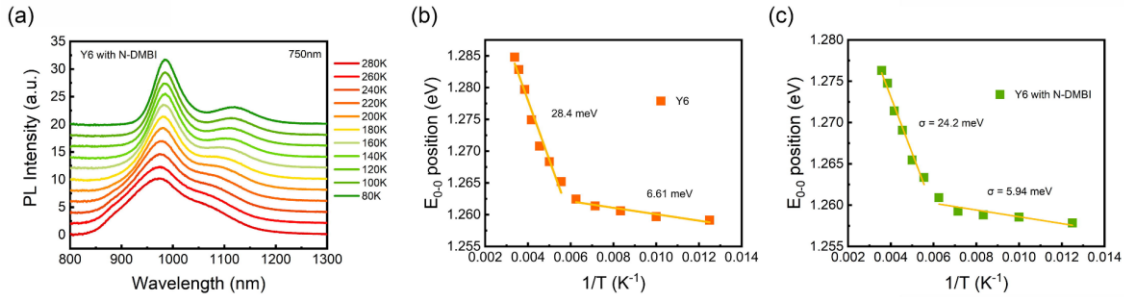

Fig. S13. (a) Temperature-dependent PL spectra for 0.1 wt% N-DMBI added Y6 film excited at 750 nm. (b-c) Temperature dependence of PL (0-0) position for the control and 0.1 wt% N-DMBI added Y6 films.

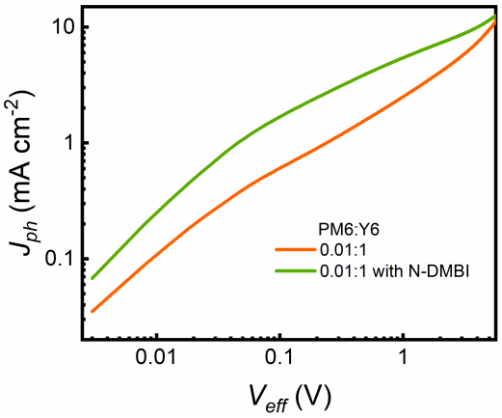

Fig. S14. J_{ph}-V_{eff} curves for the control and 0.1 wt% N-DMBI added PM6:Y6 (0.01:1) films.

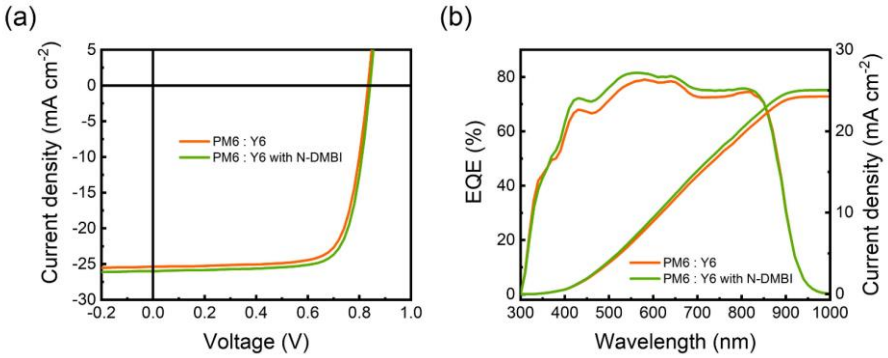

Fig. S15. (a) The *J-V* curves of the pristine and 0.01 wt% N-DMBI added PM6:Y6 BHJ devices. (b) The EQE and corresponding integrated current density curves of the pristine and 0.01 wt% N-DMBI added PM6:Y6 BHJ devices.

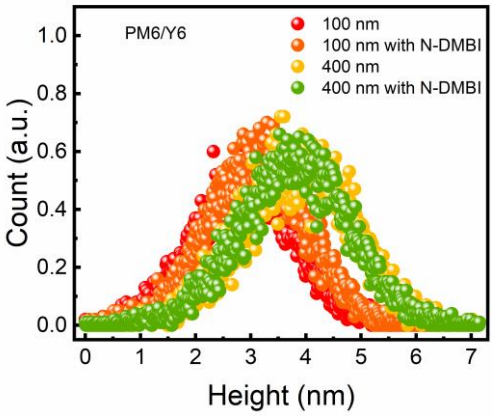

Fig. S16. Surface height histograms of the sequentially fabricated pristine and 0.01 wt% N-DMBI added PM6/Y6 BHJ films obtained by AFM.

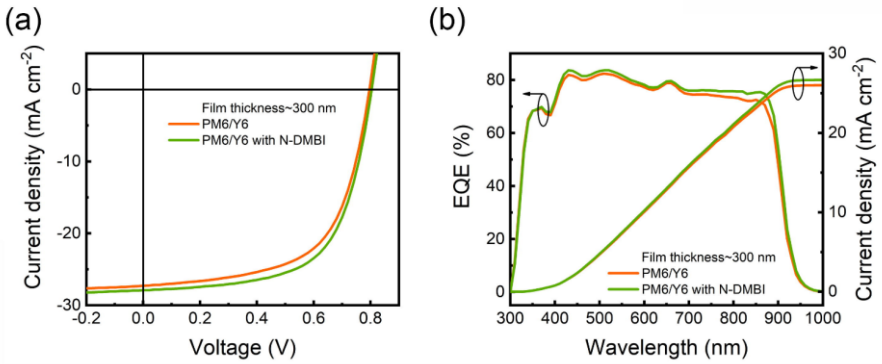

Fig. S17. (a) The *J*-*V* curves of the sequentially fabricated PM6:Y6 BHJ devices with active layer film thickness of 300 nm. (b) The EQE and corresponding integrated current density curves of the sequentially fabricated PM6:Y6 BHJ devices with active layer film thickness of 300 nm.

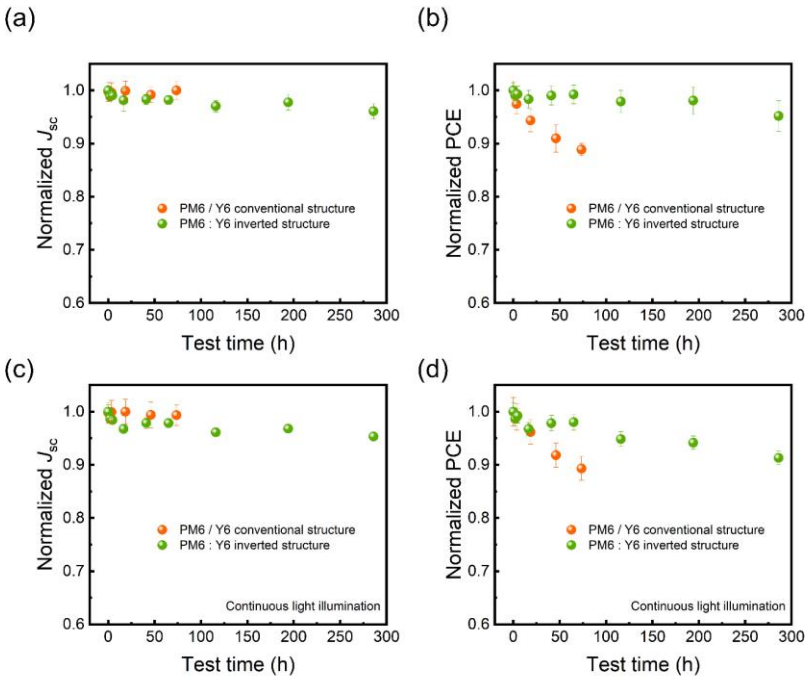

Fig. S18. (a and b) Evolution of normalized J_{sc} and PCE of sequentially fabricated PM6/Y6 BHJ devices in conventional structure and PM6 : Y6 BHJ devices in inverted structure aged without light illumination. (b and d) Evolution of normalized J_{sc} and PCE of sequentially fabricated PM6/Y6 BHJ devices in conventional structure and PM6 : Y6 BHJ devices in inverted structure aged with continuous light illumination.

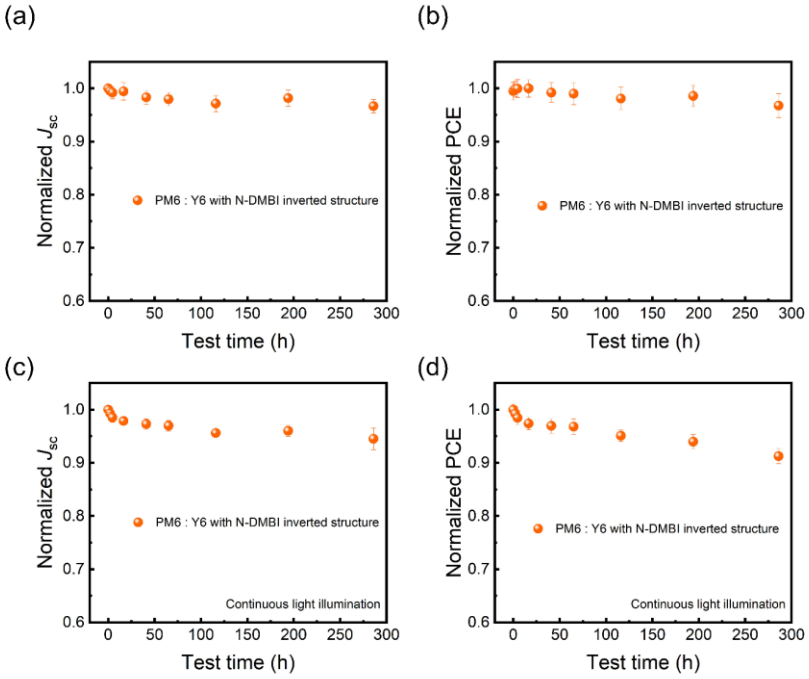

Fig. S19. (a and b) Evolution of normalized J_{sc} and PCE of inverted 0.01 wt% N-DMBI added PM6 : Y6 devices aged without light illumination. (c and d) Evolution of normalized J_{sc} and PCE of inverted 0.01 wt% N-DMBI added PM6 : Y6 devices aged with continuous light illumination.

Table S1. The ionization potential (IP), electron affinity (EA), optical gap (E_g^o), and exciton binding energy (E_b) values (in eV) of the Y6-Y6 and Y6-$Y6H^-$/N-$DMBI^+$ structures.

	IP	EA	E_g^o	E_b
Y6-Y6	6.81	2.71	2.31	1.79
Y6-$Y6H^-$/N-$DMBI^+$	4.80	2.27	1.52	1.01

Table S2. The fitted peak position and coherence length from GIWAXS patterns for the pristine and 0.1 wt% N-DMBI added PM6:Y6 (0.01:1) devices.

Materials	Location ($Å^{-1}$)	D-spacing (Å)	FWHM ($Å^{-1}$)	CL (nm)
Control	1.76	3.56	0.20	2.85
N-DMBI added	1.77	3.55	0.20	2.83

Table S3. Photovoltaic performance of PM6:Y6 (0.01:1) devices with various N-DMBI contents.[a]

Materials	N-DMBI content	$V_{oc\,max}$ (V)	$V_{oc\,avg}$ (V)	FF_{max} (%)	FF_{avg} (%)	$J_{sc\,max}$ (mA cm^{-2})	$J_{sc\,avg}$ (mA cm^{-2})	PCE_{max} (%)	PCE_{avg} (%)
PM6:Y6 (0.01:1)	0 %	0.844	0.844±0.007	33.6	33.0±0.6	2.22	2.02±0.13	0.63	0.56±0.04
	0.01 %	0.841	0.840±0.004	33.9	32.8±0.7	2.19	2.09±0.13	0.62	0.58±0.04
	0.05 %	0.858	0.845±0.010	35.7	33.8±0.7	3.44	2.95±0.32	1.05	0.84±0.10
	0.1 %	0.863	0.856±0.006	38.2	38.2±0.6	5.04	4.82±0.15	1.66	1.58±0.05
	0.3 %	0.832	0.829±0.007	30.8	30.3±0.5	2.79	2.58±0.15	0.72	0.65±0.05
	0.5 %	0.804	0.797±0.009	27.4	27.2±0.3	2.07	1.67±0.25	0.46	0.36±0.06
	1 %	0.704	0.676±0.023	27.5	27.6±0.5	2.11	1.94±0.11	0.41	0.36±0.03
	3 %	0.609	0.582±0.012	28.4	28.4±0.4	2.15	2.05±0.06	0.37	0.34±0.02

[a] The maximum and average values were obtained from more than 10 independent devices.

Table S4. Photovoltaic performance of Y6 devices with various N-DMBI contents.[a]

Materials	N-DMBI content	$V_{oc\ max}$ (V)	$V_{oc\ avg}$ (V)	FF_{max} (%)	FF_{avg} (%)	$J_{sc\ max}$ (mA cm^{-2})	$J_{sc\ avg}$ (mA cm^{-2})	PCE_{max} (%)	PCE_{avg} (%)
Y6	Control	0.855	0.841±0.011	33.9	32.3±0.9	0.26	0.25±0.01	0.08	0.07±0.00
	0.01%	0.861	0.848±0.012	32.0	32.0±0.4	0.28	0.25±0.02	0.08	0.07±0.01
	0.05%	0.864	0.854±0.009	35.0	33.6±0.9	0.29	0.27±0.02	0.09	0.08±0.01
	0.1%	0.862	0.853±0.008	33.0	31.9±0.7	0.28	0.27±0.02	0.08	0.07±0.01
	0.5%	0.870	0.868±0.007	35.9	34.4±0.9	0.33	0.30±0.02	0.10	0.09±0.01
	1%	0.879	0.876±0.012	30.5	30.6±1.2	0.37	0.33±0.04	0.10	0.09±0.01
	1.5%	0.836	0.841±0.008	23.5	24.7±0.7	0.54	0.49±0.03	0.11	0.10±0.00
	2%	0.807	0.800±0.012	23.3	22.9±0.3	0.66	0.62±0.02	0.13	0.11±0.00
	3%	0.766	0.762±0.013	22.5	23.2±0.2	0.69	0.63±0.02	0.12	0.11±0.00

[a] The maximum and average values were obtained from more than 10 independent devices.

Table S5. Summary of calculated energy loss parameters for the control and 0.1 wt% N-DMBI added PM6:Y6 (0.01:1) devices. [a]

Materials	E_g^{PV} (eV)	qV_{oc} (eV)	qV_{oc}^{SQ} (eV)	qV_{oc}^{rad} (eV)	E_g^{PV}- qV_{oc}^{SQ} (eV)	$q\triangle V_{oc}^{rad,\ below\ gap} = qV_{oc}^{SQ}$- qV_{oc}^{rad} (eV)	$q\triangle V_{oc}^{nrad} = qV_{oc}^{rad}$- qV_{oc} (eV)
Control	1.362	0.832	1.106	1.038	0.256	0.068	0.206
N-DMBI added	1.361	0.842	1.106	1.038	0.255	0.068	0.196

[a] E_g^{PV} is the photovoltaic bandgap energy, V_{oc}^{SQ} is the maximum voltage deduced by the Shockley-Queisser, V_{oc}^{rad} is the open-circuit voltage when there is only radiative recombination, $\triangle V_{oc}^{rad,\ below\ gap}$ is the voltage loss of radiative recombination from the absorption below the bandgap, $\triangle V_{oc}^{nrad}$ is the voltage loss of non-radiative recombination.

Table S6. Photovoltaic performance of PM6:L8-BO (0.01:1) devices with various N-DMBI contents.[a]

Materials	N-DMBI content	$V_{oc\ max}$ (V)	$V_{oc\ avg}$ (V)	FF_{max} (%)	FF_{avg} (%)	$J_{sc\ max}$ (mA cm^{-2})	$J_{sc\ avg}$ (mA cm^{-2})	PCE_{max} (%)	PCE_{avg} (%)
PM6:L8-BO (0.01:1)	Control	0.920	0.922±0.002	51.5	51.1±0.7	1.54	1.49±0.04	0.73	0.70±0.03
	0.01%	0.914	0.915±0.003	45.3	45.3±0.1	1.87	1.85±0.02	0.77	0.76±0.01
	0.05%	0.927	0.927±0.004	44.5	44.1±0.8	2.38	2.22±0.12	0.98	0.91±0.06
	0.1%	0.922	0.922±0.005	41.7	41.3±0.9	2.32	2.13±0.15	0.89	0.81±0.06
	0.3%	0.842	0.841±0.009	25.7	26.4±0.7	0.83	0.74±0.05	0.18	0.16±0.01

[a] The maximum and average values were obtained from more than 10 independent devices.

Table S7. Photovoltaic performance of PM6:BTP-eC9 (0.01:1) devices with various N-DMBI contents.[a]

Materials	N-DMBI content	$V_{oc\,max}$ (V)	$V_{oc\,avg}$ (V)	FF_{max} (%)	FF_{avg} (%)	$J_{sc\,max}$ (mA cm^{-2})	$J_{sc\,avg}$ (mA cm^{-2})	PCE_{max} (%)	PCE_{avg} (%)
PM6:BTP-eC9 (0.01:1)	Control	0.852	0.854±0.005	35.7	35.5±0.6	2.34	2.10±0.18	0.71	0.64±0.06
	0.01%	0.866	0.866±0.006	34.2	33.4±0.7	2.78	2.41±0.22	0.82	0.70±0.08
	0.05%	0.879	0.882±0.004	37.1	35.9±0.7	3.79	3.61±0.12	1.23	1.15±0.05
	0.1%	0.873	0.859±0.006	33.0	30.8±1.0	3.33	2.93±0.21	0.96	0.78±0.08
	0.3%	0.798	0.790±0.008	28.5	28.5±0.5	0.94	0.88±0.04	0.21	0.20±0.01

[a] The maximum and average values were obtained from more than 10 independent devices.

Table S8. Photovoltaic performance of PM6:ITIC (0.01:1) devices with various N-DMBI contents.[a]

Materials	N-DMBI content	$V_{oc\,max}$ (V)	$V_{oc\,avg}$ (V)	FF_{max} (%)	FF_{avg} (%)	$J_{sc\,max}$ (mA cm^{-2})	$J_{sc\,avg}$ (mA cm^{-2})	PCE_{max} (%)	PCE_{avg} (%)
PM6:ITIC (0.01:1)	Control	0.875	0.864±0.010	26.9	26.7±0.3	0.38	0.38±0.01	0.09	0.09±0.00
	0.05%	0.892	0.893±0.009	29.0	29.4±0.4	0.65	0.60±0.04	0.17	0.16±0.01
	0.1%	0.827	0.826±0.010	30.4	29.9±0.4	0.65	0.62±0.03	0.16	0.15±0.01
	0.3%	0.790	0.734±0.067	24.4	24.4±0.6	0.71	0.73±0.03	0.14	0.13±0.01

[a] The maximum and average values were obtained from more than 10 independent devices.

Table S9. Photovoltaic performance of PM6:IEICO (0.01:1) devices with various N-DMBI contents.[a]

Materials	N-DMBI content	$V_{oc\,max}$ (V)	$V_{oc\,avg}$ (V)	FF_{max} (%)	FF_{avg} (%)	$J_{sc\,max}$ (mA cm^{-2})	$J_{sc\,avg}$ (mA cm^{-2})	PCE_{max} (%)	PCE_{avg} (%)
PM6:IEICO (0.01:1)	Control	0.557	0.526±0.020	26.04	26.2±0.2	0.14	0.14±0.01	0.02	0.02±0.00
	0.01%	0.569	0.532±0.061	26.11	26.4±0.3	0.15	0.14±0.01	0.02	0.02±0.00
	0.05%	0.627	0.563±0.055	25.99	26.3±0.3	0.17	0.15±0.02	0.03	0.02±0.00
	0.1%	0.844	0.835±0.010	28.71	28.2±0.6	0.27	0.24±0.02	0.06	0.06±0.01
	0.3%	0.865	0.861±0.007	28.44	28.3±0.2	0.75	0.75±0.03	0.19	0.18±0.01
	0.5%	0.776	0.732±0.036	26.67	27.2±0.6	1.19	1.17±0.02	0.25	0.23±0.01
	1%	0.068	0.052±0.013	25.31	24.4±0.7	0.32	0.34±0.02	0.01	0.00±0.00

[a] The maximum and average values were obtained from more than 10 independent devices.

Table S10. Photovoltaic performance of PM6:Y6 (0.01:1) devices with various DMBI-BDZC and TBAI contents.[a]

Materials		$V_{oc\,max}$ (V)	$V_{oc\,avg}$ (V)	FF_{max} (%)	FF_{avg} (%)	$J_{sc\,max}$ (mA cm^{-2})	$J_{sc\,avg}$ (mA cm^{-2})	PCE_{max} (%)	PCE_{avg} (%)
PM6:Y6 (0.01:1)	0.01% DMBI-BDZC	0.838	0.835±0.007	39.2	39.0±0.6	3.12	3.04±0.11	1.03	0.99±0.03
	0.05% DMBI-BDZC	0.846	0.842±0.003	40.1	39.4±0.6	3.50	3.17±0.19	1.18	1.05±0.08
	0.1% DMBI-BDZC	0.849	0.845±0.004	38.7	38.8±0.3	4.32	4.08±0.27	1.42	1.34±0.08
	0.3% DMBI-BDZC	0.837	0.838±0.005	38.2	37.9±0.7	2.84	2.76±0.15	0.91	0.88±0.05
	0.01% TBAI	0.846	0.844±0.004	36.4	35.6±0.6	3.10	2.72±0.24	0.95	0.82±0.08
	0.05% TBAI	0.851	0.851±0.005	35.2	33.3±1.0	4.69	4.41±0.24	1.40	1.25±0.10
	0.1% TBAI	0.832	0.830±0.008	29.8	28.9±0.8	3.47	3.18±0.14	0.86	0.76±0.06
	0.3% TBAI	0.732	0.717±0.013	24.4	24.0±0.4	2.32	2.25±0.08	0.41	0.39±0.02

[a] The maximum and average values were obtained from more than 10 independent devices.

Table S11. Mobility data of the control and 0.1 wt% N-DMBI added PM6:Y6 (0.01:1) films.

Materials	Electron mobility (10^{-4} cm^{2}V^{-1}s^{-1})	Hole mobility (10^{-4} cm^{2}V^{-1}s^{-1})
0.01:1	0.87±0.16	2.67±1.38
0.01:1 N-DMBI added	1.42±0.46	1.50±0.59

Table S12. Photovoltaic performance of sequentially fabricated PM6 (50 nm)/Y6 (10mg/ml, 4000 rpm for 30s) BHJ devices with active layer film thickness of 100 nm.[a]

Materials	N-DMBI content	$V_{oc\,max}$ (V)	$V_{oc\,avg}$ (V)	FF_{max} (%)	FF_{avg} (%)	$J_{sc\,max}$ (mA cm^{-2})	$J_{sc\,avg}$ (mA cm^{-2})	PCE_{max} (%)	PCE_{avg} (%)
PM6/Y6	0 %	0.823	0.824±0.003	75.9	75.5±1.0	25.62	25.23±0.37	16.09	15.75±0.18
	0.005 %	0.831	0.825±0.004	76.6	76.0±0.6	25.59	25.30±0.22	16.36	15.94±0.23
	0.01 %	0.829	0.827±0.003	75.9	75.6±0.7	26.43	26.06±0.46	16.70	16.36±0.19
	0.05 %	0.828	0.825±0.004	75.6	75.5±0.8	26.04	25.49±0.39	16.37	15.94±0.27
	0.1 %	0.814	0.810±0.004	72.4	71.5±0.9	25.87	25.43±0.32	15.25	14.75±0.32

[a] The maximum and average values were obtained from 10 independent devices.

Table S13. Photovoltaic performance of PM6:Y6 BHJ devices with various N-DMBI contents.[a]

Materials	N-DMBI content	$V_{oc\,max}$ (V)	$V_{oc\,avg}$ (V)	FF_{max} (%)	FF_{avg} (%)	$J_{sc\,max}$ (mA cm^{-2})	$J_{sc\,avg}$ (mA cm^{-2})	PCE_{max} (%)	PCE_{avg} (%)	EQE (mA cm^{-2})
PM6 : Y6	0%	0.834	0.835±0.003	75.1	75.1±0.5	25.37	25.06±0.17	15.89	15.73±0.09	24.28
	0.005%	0.842	0.837±0.003	75.9	76.2±0.6	25.53	25.22±0.23	16.31	16.10±0.11	
	0.01%	0.841	0.838±0.003	75.8	75.8±0.6	25.98	25.76±0.20	16.56	16.35±0.15	25.06
	0.05%	0.837	0.838±0.003	75.5	75.6±0.7	25.78	25.48±0.34	16.28	16.15±0.09	

[a] The maximum and average values were obtained from more than 10 independent devices.

Table S14. Photovoltaic performance of sequentially fabricated PM6 (130 nm)/Y6 (15 mg/ml, 2500 rpm for 30s) BHJ devices with active layer film thickness of 300 nm.[a]

Materials	N-DMBI content	$V_{oc\,max}$ (V)	$V_{oc\,avg}$ (V)	FF_{max} (%)	FF_{avg} (%)	$J_{sc\,max}$ (mA cm^{-2})	$J_{sc\,avg}$ (mA cm^{-2})	PCE_{max} (%)	PCE_{avg} (%)
PM6/Y6	0 %	0.796	0.796±0.004	61.0	60.2±0.9	27.28	27.05±0.23	13.31	13.03±0.17
	0.001 %	0.796	0.796±0.003	62.1	61.4±0.7	27.29	27.28±0.18	13.55	13.38±0.22
	0.005 %	0.800	0.799±0.003	62.4	62.1±0.5	27.52	27.45±0.25	13.80	13.67±0.08
	0.01 %	0.804	0.799±0.003	62.9	62.5±0.5	27.90	27.64±0.24	14.19	13.86±0.19
	0.05 %	0.807	0.799±0.005	62.5	62.2±0.6	27.54	27.35±0.10	13.96	13.67±0.14

[a] The maximum and average values were obtained from 10 independent devices.

Table S15. Photovoltaic performance of sequentially fabricated PM6 (180 nm)/Y6 (15 mg/ml, 1300 rpm for 30s) BHJ devices with active layer film thickness of 400 nm.[a]

Materials	N-DMBI content	$V_{oc\,max}$ (V)	$V_{oc\,avg}$ (V)	FF_{max} (%)	FF_{avg} (%)	$J_{sc\,max}$ (mA cm^{-2})	$J_{sc\,avg}$ (mA cm^{-2})	PCE_{max} (%)	PCE_{avg} (%)
PM6/Y6	0%	0.794	0.794±0.004	56.7	55.7±1.0	26.51	26.25±0.36	11.88	11.62±0.28
	0.005%	0.797	0.796±0.004	57.0	57.1±0.5	27.12	26.82±0.20	12.34	12.18±0.13
	0.01%	0.798	0.799±0.003	58.4	57.4±0.6	27.91	27.59±0.20	13.03	12.63±0.17
	0.05%	0.796	0.798±0.004	57.0	57.0±0.6	27.44	26.95±0.31	12.46	12.23±0.19
	0.1%	0.798	0.799±0.004	58.2	57.3±0.7	25.23	25.15±0.32	11.67	11.47±0.24

[a] The maximum and average values were obtained from 10 independent devices.

Supplemental references

1. A. Hexemer, W. Bras, J. Glossinger, E. Schaible, E. Gann, R. Kirian, A. MacDowell, M. Church, B. Rude, H. Padmore, *J. Phys. Conf. Ser.* 2010, **247**, 012007.
2. G. Han, T. Hu and Y. Yi, *Adv. Mater.* 2020, **32,** 2000975.
3. J.-D. Chai and M. Head-Gordon, *Phys. Chem. Chem. Phys.* 2008, **10,** 6615-6620.
4. P. J. Hay and W. R. Wadt, *J. Chem. Phys.* 1985, **82,** 284-298.
5. W. J. Hehre, R. Ditchfield and J. A. Pople, *J. Chem. Phys.* 1972, **56,** 2257-2261.
6. R. Ditchfield, W. J. Hehre and J. A. Pople, *J. Chem. Phys.* 1971, **54,** 724-728.
7. P. C. Hariharan and J. A. Pople, *Theoret. chim. Acta* 1973, **28,** 213-222.
8. J.-L. Bredas, J. Cornil and A. J. Heeger, *Adv. Mater.* 1996, **8,** 447-452.
9. M. Knupfer, *Appl. Phys. A: Mater. Sci. Process.* 2003, **77,** 623-626.
10. A. Dkhissi, *Synth. Met.* 2011, **161,** 1441-1443.
11. P. K. Nayak, *Synth. Met.* 2013, **174,** 42-45.
12. B. M. Savoie, N. E. Jackson, L. X. Chen, T. J. Marks and M. A. Ratner, *Acc. Chem. Res.* 2014, **47,** 3385-3394.
13. Gaussian.; A. Revision, M. J. Frisch, G. W. Trucks, H. B. Schlegel, G. E. Scuseria, M. A. Robb, J. R. Cheeseman, G. Scalmani, V. Barone, G. A. Petersson, H. Nakatsuji, X. Li, M. Caricato, A. V. Marenich, J. Bloino, B. G. Janesko, R. Gomperts, B. Mennucci, H. P. Hratchian, J. V. Ortiz, A. F. Izmaylov, J. L. Sonnenberg, D. Williams-Young, F. Ding, F. Lipparini, F. Egidi, J. Goings, B. Peng, A. Petrone, T. Henderson, D. Ranasinghe, V. G. Zakrzewski, J. Gao, N. Rega, G. Zheng, W. Liang, M. Hada, M. Ehara, K. Toyota, R. Fukuda, J. Hasegawa, M. Ishida, T. Nakajima, Y. Honda, O. Kitao, H. Nakai, T. Vreven, K. Throssell, J. A. Montgomery, Jr. J. E. Peralta, F. Ogliaro, M. J. Bearpark, J. J. Heyd, E. N. Brothers, K. N. Kudin, V. N. Staroverov, T. A. Keith, R. Kobayashi, J. Normand, K. Raghavachari, A. P. Rendell, J. C. Burant, S. S. Iyengar, J. Tomasi, M. Cossi, J. M. Millam, M. Klene, C. Adamo, R. Cammi, J. W. Ochterski, R. L. Martin, K. Morokuma, O. Farkas, J. B. Foresman and D. J. Fox, (2016). Gaussian, Inc., Wallingford CT, 2016.
14. J. Benduhn, K. Tvingstedt, F. Piersimoni, S. Ullbrich, Y. Fan, M. Tropiano, K. A. McGarry, O. Zeika, M. K. Riede, C. J. Douglas, S. Barlow, S. R. Marder, N. Neher, D. Spoltore and K. Vandewal, *Nat. Energy* 2017, **2,** 17053.
15. J. Liu, S. Chen, D. Qian, B. Gautam, G. Yang, J. Zhao, J. Bergqvist, F. Zhang, W. Ma, H. Ade, O. Inganäs, K. Gundogdu, F. Gao and H. Yan, *Nat. Energy* 2016, **27,** 16089.
16. Y. Tamai, H. Ohkita, H. Benten and S. Ito, *J. Phys. Chem. Lett.* 2015, **6,** 3417-3428.
17. D. E. Markov, E. Amsterdam, P. W. M. Blom, A. B. Sieval and J. C. Hummelen, *J. Phys. Chem. A* 2005, **109,** 5266-5274.
18. D. E. Markov, C. Tanase, P. W. M. Blom and J. Wildeman, *Phys. Rev. B* 2005, **72,** 045217.

19. Y. Firdaus, V. M. L. Corre, S. Karuthedath, W. Liu, A. Markina, W. Huang, S. Chattopadhyay, M. M. Nahid, M. I. Nugraha, Y. Lin, A. Seitkhan, A. Basu, W. Zhang, I. McCulloch, H. Ade, J. Labram, F. Laquai, D. Andrienko, L. J. A. Koster and T. D. Anthopoulos, *Nat. Commun.* 2020, **11,** 5220.
20. B. Siegmund, M. T. Sajjad, J. Widmer, D. Ray, C. Koerner, M. Riede, K. Leo, I. D. W. Samuel and K. Vandewal, *Adv. Mater.* 2016, **29,** 1604424.
21. S. Yoo, B. Domercq and B. Kippelen, *Appl. Phys. Lett.* 2004, **85,** 5427.
22. P. Pattanasattayavong, G. O. N. Ndjawa, K. Zhao, K. W. Chou, N. Yaacobi-Gross, B. C. O'Regan, A. Amassian and T. D. Anthopoulos, *Chem. Commun.* 2013, **49,** 4154.
23. R. Kerremans, C. Kaiser, W. Li, N. Zarrabi, P. Meredith and A. Armin, *Adv. Optical Mater.* 2020, **8,** 2000319.